CHAPTER 2

EXPERIMENTAL

The combination of solid state materials science with thin film technology has significantly reduced the sizes of the electronic components/devices for various scientific and technological applications from console to portable and then to miniaturization. The microelectronic circuit technology requires several types of thin films for a variety of applications. These coatings can be single or multicomponet, alloy/compound or mulitlayer type on substrates of different nature, size and shapes. A large variety of deposition techniques have been developed to obtain thin films of different types of materials. The principles of the different deposition techniques, their advantages and limitations are described in detail in the literature [1-5]. The properties and the application of a thin film depends on its preparation history like method of deposition and the deposition conditions like vacuum, deposition rate, temperature, substrate material, source temperature, source-substrate distance, partial pressure of the residual gases during deposition etc. The thin film characterization is also very important for device application as the properties strongly depend on the deposition parameters.

This chapter deals with the various preparation and characterization techniques used in the present investigation. The dc magnetron sputtering technique was used for the preparation of Cu_2O and $CuAlO_2$ thin films.

Cu_2O and $CuAlO_2$ thin films have been prepared mostly by wet process like thermal oxidation [6], electrodeposition [7,8], sol-gel process [9,10], solution growth [11], electron beam evaporation [12,13], chemical vapor deposition [14,15], filtered cathodic vacuum arc deposition [16], pulsed laser deposition [17,18], activated reactive evaporation [19], dip-coating [20], spin-on technique [21] and sputtering [22-25].

Among these techniques, dc reactive magnetron sputtering is one of the most useful techniques for the preparation of thin films. Sputtering has become one of the most versatile techniques in thin film technology. Using sputtering techniques, almost all materials are prepared in thin film form. The main features of sputtering process are

(i) High uniformity thickness of the deposited films.

(ii) Good adhesion to the substrate.

(iii) There is no direct heating of the material.

(iv) No reaction between the evaporated material and the source as in thermal evaporation.

(v) Better reproducibility of films.

(vi) Ability of the deposit to maintain the stoichiometry of the original target composition.

(vii) Relative simplicity of film thickness control item.

(viii) It is important for alloy and compounds.

SPUTTERING PROCESS

Sputtering is a fairly new technology in the semiconductor industry. This technique was discovered in 1852 by Grove [26]. Sputtering is a process operating on atomic or molecular scale where an atom or molecule of a surface is ejected when the surface is struck by a fast incident particle. The momentum of the incident atom is transferred to the atoms in the target material and this momentum transfer can often lead to the ejection of a surface atom. Fig.2.1 shows the schematic diagram of sputtering process. Depending on the ion source, two techniques namely ion beam sputtering and glow discharge sputtering have been developed, among which glow discharge sputtering

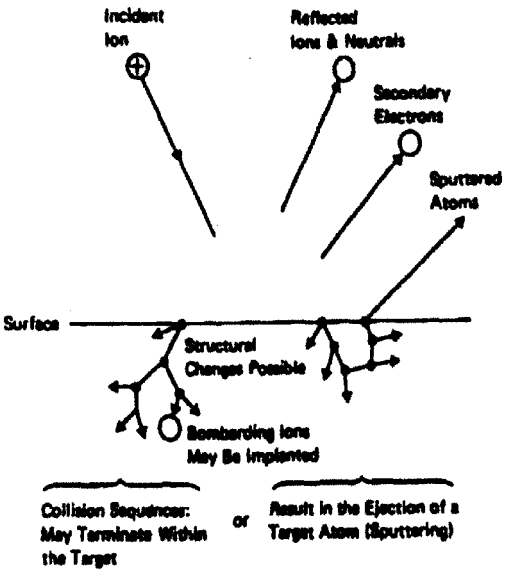

Fig.2.1 The Sputtering progress (Chapman 1980)

was found to be the most convenient because of the precise control of the chemical composition and physical properties of the films using a large number of sputtering parameters. The sputtering yield, the most important parameter for characterizing the sputtering process, is defined as the number of atoms ejected from the target surface per incident ion, depends on the bombarded material, its structure and composition, the characteristics of the incident ion, and also experimental geometry.

2.1 Glow discharge dc sputtering

The schematic diagram of glow discharge dc sputtering is shown in Fig.2.2. The glow discharge can be set up by applying either a dc or rf voltage between the sputter target and the substrate. A plate of the material to be deposited (target) is connected to

negative voltage supply and the substrate facing the target is mounted on the adjacent anode. A neutral gas such as argon is introduced into the vacuum chamber upto pressure of $10^{-1} - 10^{-2}$ mbar. An electric field is applied between the two electrodes. The electric

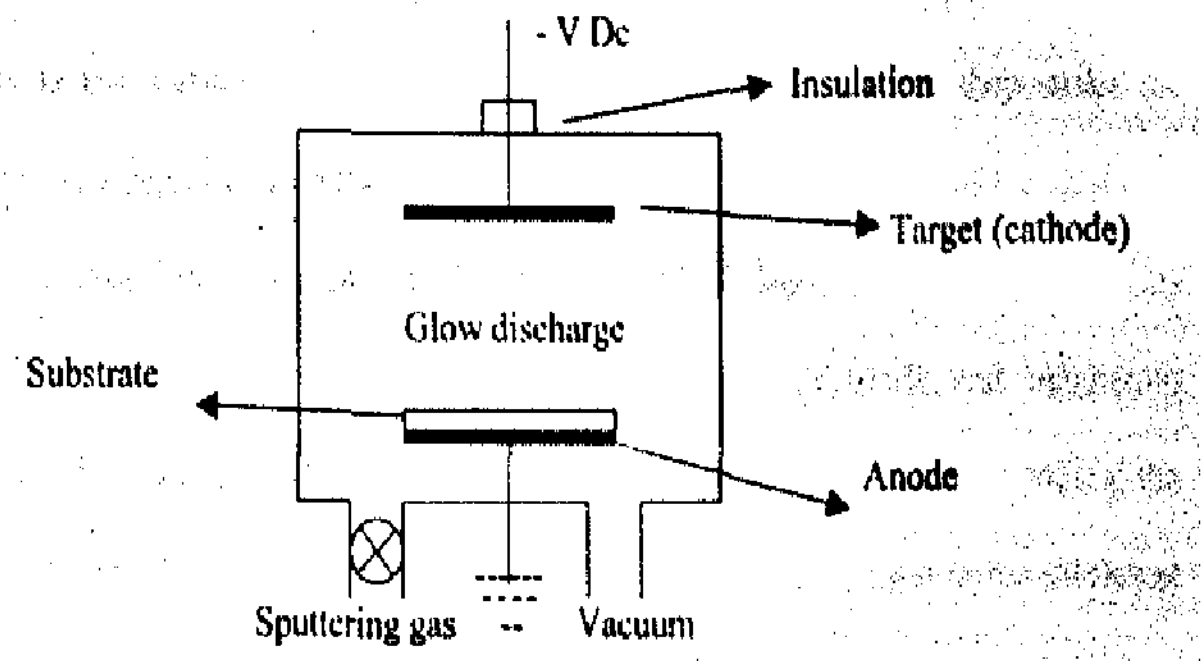

Fig.2.2 Schematic of simplified Dc sputtering system.

filed causes electrons to be accelerated. These electrons collide with neutral atoms, causing ionization and the generation of ions and electrons. These new electrons are then accelerated by the electric field and produce more positive ions. The positive ions strike the target and remove the neutral atoms from the surface of the target, eventually condense as a thin film on the substrate. Electrons are also emitted from the target by ion bombardment and these are accelerated towards the substrate platform, when they collide with the gas atoms. These electrons help to maintain the glow discharge. If the gas pressure is too low or the cathode anode spacing too small, the secondary electrons can not under go sufficient ionizing collisions before they hit the anode, on the other hand, if the pressure and/or separation is too large, the ions generated are slowed by inelastic collisions, and when they strike the target, they will not have enough energy to produce

secondary electrons. Missel [27] has suggested that the optimum conditions for ensuring uniformity of the deposition. In a practical sputtering system, the self-sustained dc discharge can not be sustained at a pressure below 10 mbar because there are insufficient ionizing collisions. Another advantage that might be expected from sputtering at low pressure is the higher mean energy of the sputtering particles when they strike the substrate, resulting in better adhesion of the films. The deposition rate of the sputtered films is usually low when compared with other films deposition techniques. This disadvantage could be avoided only after the invention of triode and magnetron sputtering. In triode sputtering, due to the presence of an additional electron source, the ionization in the discharge can be increased. The increased ionization in the discharge led to an increase in the rate of sputtering and hence the deposition rate. In magnetron sputtering, increasing the path length between the substrate and the target increase the ionizing efficiency of the electrons. Applying a magnetic field either longitudinally or transversely to the inter-electrode spacing can enhance the path length of the electrons.

2.2 Magnetron sputtering

Magnetron sputtering technology was introduced in the 1930's primarily by Penning and his contemporaries [28]. This technology has made significant progress since its development and it was developed substantially by Penfold and Thornton [29] for the high rate deposition of metal, semiconductor and dielectric films. High deposition rates at lower operating pressures, make it possible to obtain high quality films at low substrate temperatures. The planar magnetron sputtering was introduced in 1974 by

Chapin [30] although the basic principle of a planar magnetron device had been demonstrated in 1959 by Kesaer and Pashkova [31]. In sputtering discharges, the sputtering rate depends directly on the ion flux, and this in turn depends on the density of ions in the plasma. The use of magnetic field is primarily to trap electrons close to the sputtering target, so as both to prevent them from escaping to the walls where they will cause ion loss by recombination but also to create ions by electron impact close to the sputtering target.

The interaction between the magnetic field B and an electron with vector velocity 'V' given by

$$F = eV \times B \qquad \text{-----(1)}$$

where 'F' is the force, is in a direction orthogonal to both the magnetic filed and electron velocity vectors (see in Fig.2.3). As a result, there is a strong tendency for the electron to travel in helical motion close to the target surface where both the magnetic field strength and the electron velocity are large. By this means of magnetic enhancement, ion flux can be increased to several tens of milliamps per square centimeter, with corresponding increase in deposition rates.

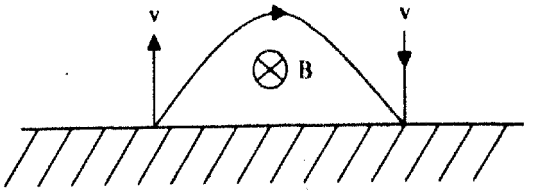

$$r = \frac{m_e v}{B_e}$$

Fig.2.3 The influence of a magnetic field on electron motion (Chapman 1980).

On the other hand, permanent magnets like barium and strontium ferrites, AlNiCo and rare earth samarium cobalt magnets have been widely used. The basic condition in choosing the magnets is that the transverse component of the magnetic field in front of the target is typically in the range of 200-500 Gauss, though the threshold magnetic field for achieving magnetron discharge is as low as 90 Gauss [32]. Higher magnetic field will result in lowering of the operating pressure. The high discharge current density is possible in a magnetron cathode leads to excessive heating of the target and hence a cooling system is necessary. The surface temperature of the target of 1 cm thickness would be 720 °C if the power density was 10 W/cm^2 [33]. This provides an additional source of substrate heating and could have deleterious effects on the target. Limited water cooling of the target will eventually limit the power that can be dissipated and thus the sputtering rate can be obtained. Most of the ion energy that reaches the target is dissipated there as heat. So efficient water cooling of the target is necessary to maintain the target at low temperatures. Otherwise, the possible adverse effects such as the target may be damaged, a hot target will also cause the substrate heating through thermal radiation and out gassing will occur.

Most magnetron source operates in the pressure range from 1 mbar to 20 mbar and a cathode potential of 300 – 700 V. The sputtering rates are primarily determined by the ion current density at the target, and the depositing rates are affected by factor such as applied power, source to substrate distance, target material, partial pressure, sputtering pressure, substrate temperature etc.

In magnetron sputtering, the following parameters influence the film properties by carefully adjusting these parameters, good quality films will be deposited. The parameters are

----- Sputtering current (Isp)

----- The base Pressure (P)

----- The gas mixture

----- The substrate temperature (Ts)

----- Bias voltage (V_b)

The sputter current (Isp) determines mainly the rate of the deposition process and hence the time which remains for the arriving particles during the growth process for either surface diffusion and agglomeration on existing growth centers or nucleation with other adatoms. The applied voltage determines the maximum energy, with which sputtered particles can escape from the target (reduced by the binding energy). Energies of the sputtered particles show a broad distribution with a maximum of the distribution between 1-10 eV. The applied voltage determines also the sputter yield.

The pressure (p) in the sputter chamber determines the mean free path λ for the sputtered material, which is proportional to 1/p. Together with the target to substrate distance (T-S), the pressure controls the number of collisions occur for the particles on their way from target to substrate. This can influence the porosity of the films, which in turn influence the crystallinity and texture. Using a desirable gas mixture of oxygen and argon can control the stoichiometry of films.

The substrate temperature can have a strong impact on the growth behaviour with respect to crystallinity or density of the films. It can be adjusted between room temperature and 500 °C (for glass substrate). But even during sputtering without external heating the substrate temperature may rise considerably, especially during long sputtering times for the deposition of thick films.

Bias-voltage can be applied to the substrate up to ±100V, which has the effect of accelerating electrons or ions towards the substrate or keeping them away.

Usually substrate and target surface are parallel to each other. A variation of the deposition angle (also: sputtering under oblique incidence) can be achieved by tilting the substrate. Thereby a new preferential direction for the film growth and potentially anistorpic films can be produced.

The main features of magnetron sputtering

- High rate of sputtering due to the confinement of the plasma close to the target surface.
- Sputtering can takes place at a low gas pressure due to the increased path length of electrons within the plasma and prevention of their escape.
- High rate of material removal from the target occurs when the magnetic field lines are parallel to the cathode surface.
- The target utilization in most of the magnetron targets is about 30 %.

2.3 Reactive sputtering

Reactive sputtering was developed in the 1950s by Westwood [34]. Reactive sputtering is the sputtering of an elemental target in the presence of a gas that will react

with the target material to form a compound. Reactive sputtering has proliferated, particularly over the past few decades. It is used extensively by manufacturers of coated architectural glass roll or web coatings, coated cutting tools, optical coatings, decarative and functional coatings for plumbing and hard ware items, microelectronic devices, surface acoustic wave devices, and transparent conducting oxides etc. In one sense all sputtering is reactive because there are always residual gases in the chamber that will react with the sputtered species. However in reality, reactive sputtering occurs when a gas is purposely added to the sputtering chamber to react with the sputtered material. Reactive gases like oxygen or nitrogen are introduced into the system along with the inert gas to deposit oxides or nitrides. In reactive sputtering, one important problem is that the metallic sputtering target may become oxidized by the reactive gas. The oxidation of the metallic sputtering target during reactive sputtering may occur by collision of oxygen species from the plasma with the target or by chemisorption of oxygen followed by oxidation.

When a metal is sputtered in the presence of a reactive gas, the three possible locations at which reaction between sputtered atoms and reactive gas takes place at any or all of three locations: (1) at the target (2) in the gas phase (3) on the substrate surface. When the reaction takes place at the target surface, an insulating film formed on the target would terminate the process if a dc discharge was employed, or would often slow it down in an rf discharge. Reaction in the gas phase often will lead to the further agglomeration or nucleation of the resulting molecules so that the material arrives at the substrate in large particles or powder, producing a finable coating of limited utility.

Normally way of reaction is on the substrate surface. In order to accomplish this effectively, the process must be well controlled. The reaction during transport may not be possible due to momentum and energy conservation effects and as such the most probable location is near the substrate or the target. The phase of the compound film formed depends on both the percentage of the reactive gas in the sputtering environment and on the reduce field E* defined as

$$E^* = \frac{\text{cathode voltage}}{\text{Target-substrate distance x Pressure}} \qquad \text{-----(2)}$$

The significance of E* is that the energy of the negative ions originating at the cathode is supposed to be proportional to it and thereby strongly influence the re-emission coefficient [35]. Therefore, E* is important in controlling the particular phase grown.

In reactive sputtering, the target may become an insulating one when the rate of sputtering is less than the rate at which the reactive gas atoms reach the target. This is often termed as the target poisoning and it leads to undesirable effects like, drastic drop in deposition rate and extinction of the glow discharge itself. However, with the advent of magnetron sputtering the situation has become quite different. Due to high deposition rate, the critical pressure of the reactive gas at which the target poisoning takes place can be high. The immediate consequence of this is that the decomposition of the deposited film can be varied.

2.4 Dc magnetron sputtering system

A dc reactive magnetron sputtering system was developed in the laboratory for the deposition of Cu_2O and $CuAlO_2$ films. The diagram of the sputtering system is shown in Fig.2.4. It consists of a vacuum chamber (both ends open) made up of stainless

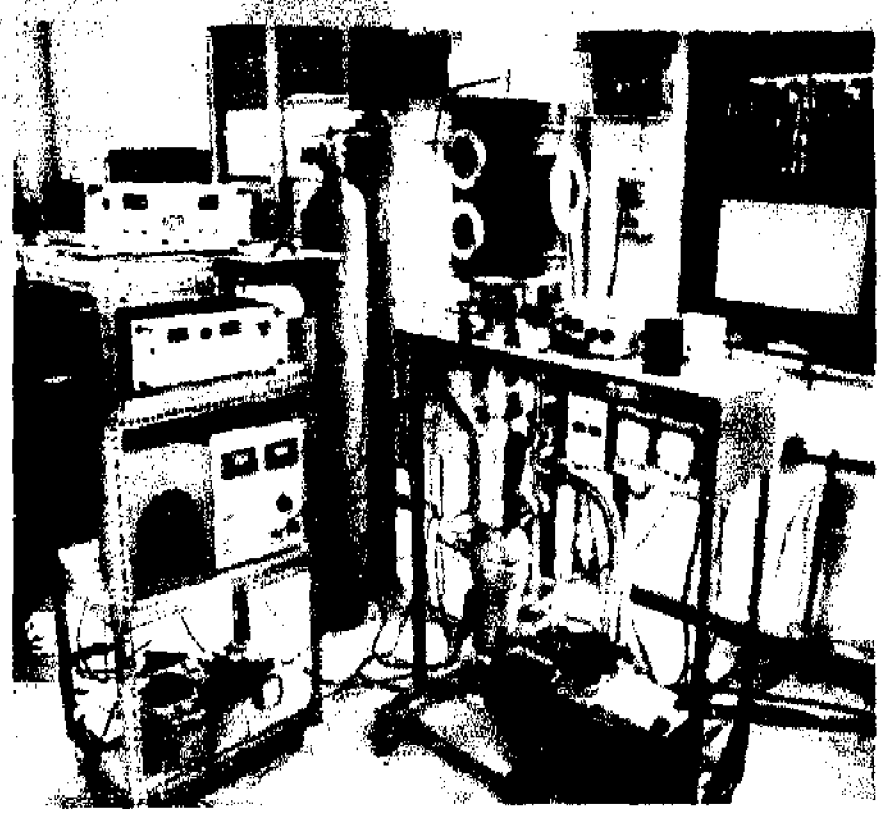

Fig.2.4 Experimental setup of the dc magnetron sputtering system

steel with 290 mm diameter and 350 mm height. The magnetron target assembly is mounted to the top plate (using Teflon as electric insulation) such that the sputtering can be performed in sputter down mode. The schematic of the planar magnetron target assembly designed and constructed in the laboratory is shown in Fig.2.5. A circular planar magnetron of 100 mm diameter was used as the magnetron cathode. The magnetron has been designed in such a way that two permanent ring magnets made of samarium cobalt, one of 10 mm diameter and the other of 54 mm diameter are kept

concentrically under the target plate and are always water cooled. The samarium cobalt magnets are coated with a thin layer of lacquer prior to fixing them inside the planar target to prevent corrosion of the magnets due to water circulation inside the target. The vacuum chamber is pumped using a diffusion pump (300 lit/min), which is backed by a direct drive rotary pump (200 lit/min). A liquid nitrogen trap incorporated between the chamber and the diffusion pump minimized the oil vapour contamination on the chamber.

The system gives an ultimate vacuum of about $1x10^{-6}$ mbar. Pure argon was used as

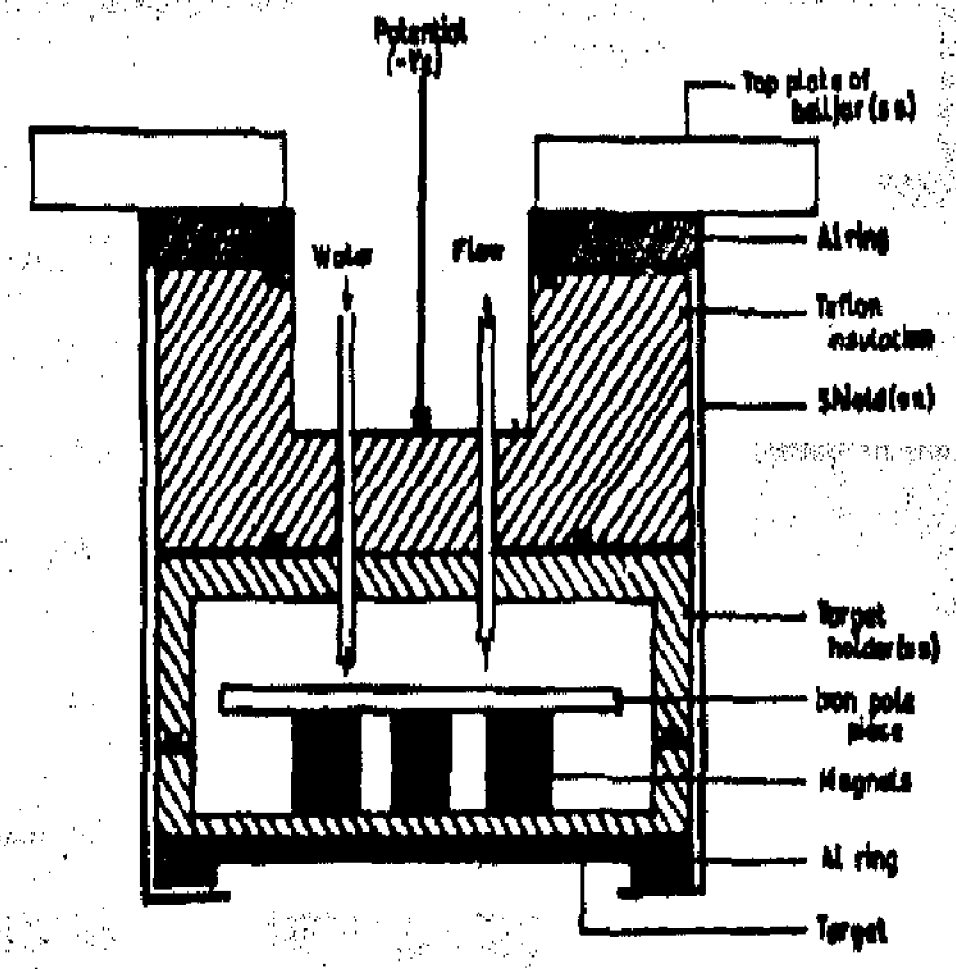

Fig.2.5 Schematic of planar magnetron target assembly.

sputter gas and oxygen as reactive gas. Pure oxygen gas was admitted into the chamber through the needle valve and the required oxygen partial pressure was set and allowed to stabilize. Argon gas was then introduced and the required sputtering pressure was maintained. The flow rates of both argon and oxygen gases were controlled individually

by Tylan mass flow controllers (Model FC-260). A continuously variable dc power supply of 750 V and 3 A was used as a power source for sputtering. Before deposition of each film, the target was sputtered in pure argon atmosphere for 15 min to remove oxide layers if any on the surface of the target. The substrates were kept parallel to the target at a distance of 65 mm. An iron-constantan thermocouple placed in contact with the substrate surface was used to monitor the substrate temperature. A feedback controlled heater controls the substrate temperature. The substrates were maintained at the required temperature to an accuracy of ± 5 °C.

Glow discharge characteristics of the magnetron

In order to study the performance of the fabricated magnetron sputtering, the cathode current-voltage (I-V) and the cathode voltage sputtering pressure characteristics have been studied systematically. The current-voltage relationship in the magnetron followed the relation,

$$I = KV^n \qquad \text{-----(3)}$$

Where 'n' is a constant representing the efficiency of the electron trapping in the plasma and 'k' is a constant [36].

2.5 Target erosion and film uniformity

Fig.2.6. shows the erosion pattern for the planar magnetron cathode. The planar magnetron behaves essentially as a ring source owing to the shape of the confined plasma. It was observed that erosion takes place in the region where the magnetic field is parallel to the target surface.

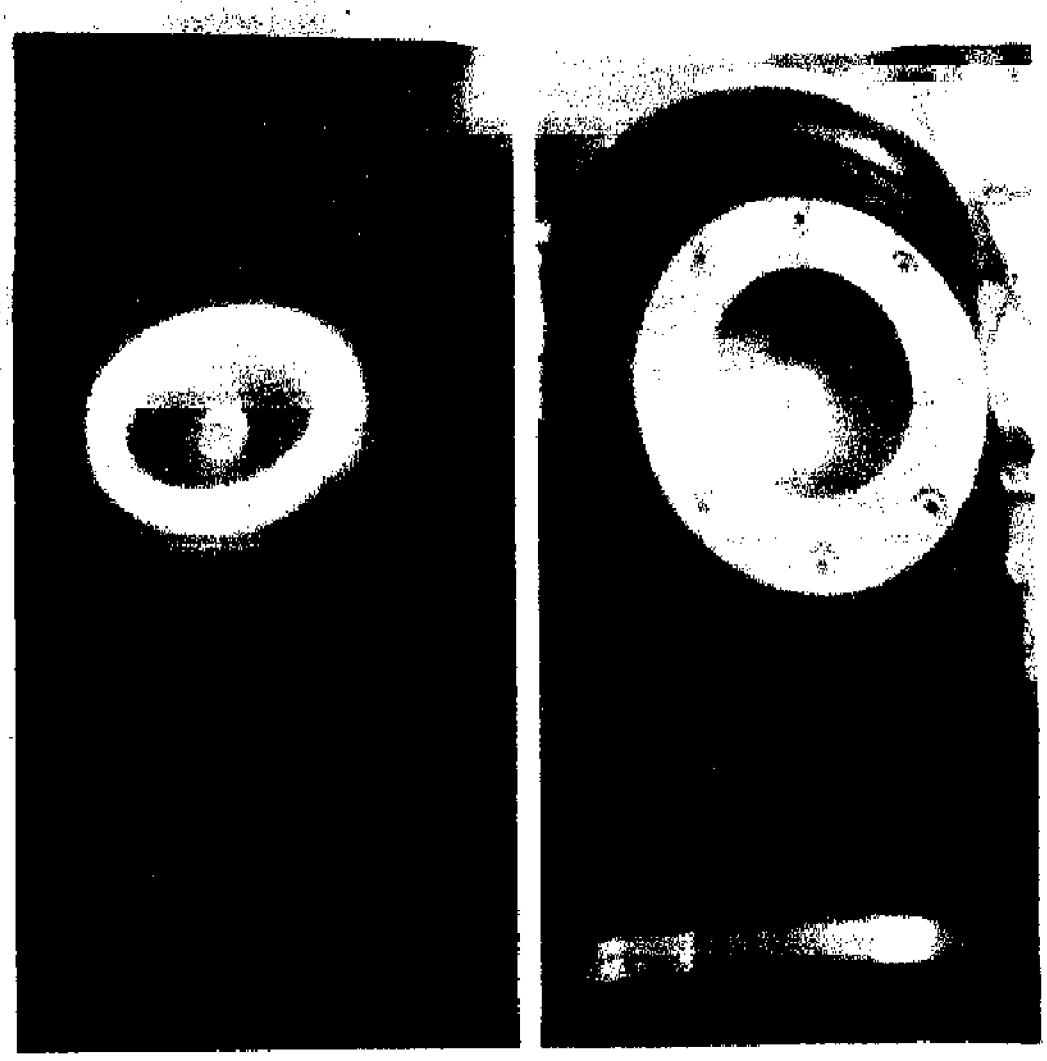

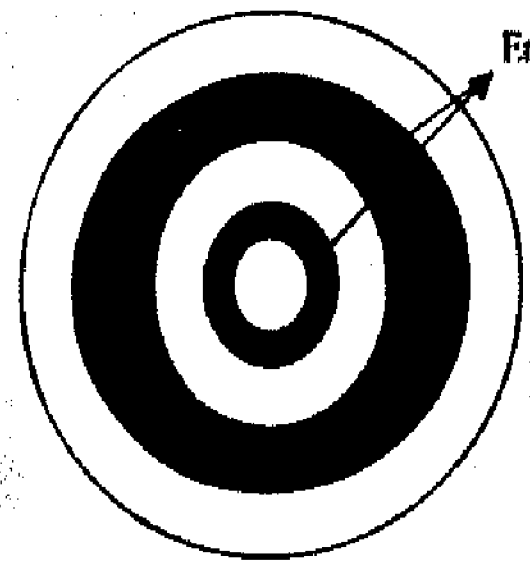

Fig.2.6 shows the erosion pattern for the planar magnetron cathode

PREPARATION OF Cu_2O AND $CuAlO_2$ FILMS

The dc reactive magnetron sputtering system developed in the laboratory was used for the preparation of Cu_2O and $CuAlO_2$ films. Thin films of Cu_2O and $CuAlO_2$ have been prepared under various oxygen partial pressures, substrate temperatures, sputtering powers, sputtering pressures and substrate bias voltages. The system was arranged in a sputter down configuration with a substrate to target spacing of 65 mm. Corning 7059 glass substrates were used as the substrates.

2.6 Substrate Cleaning

Cleanliness of the substrate surface directly influence the film growth and adhesion. This in turn strongly manipulates the properties of the thin films such as microstructure, surface topography and other mechanical properties. Also a meticulously cleaned substrate is a prerequisite for preparation of thin films with repeatable properties. Corning 7059 glass substrates were used for the deposition of Cu_2O films and $CuAlO_2$ films. The systematic procedure adopted for cleaning the substrates are outlined in the following steps.

- The glass substrates were cleaned at first by mild soap solution
- Then washed thoroughly in deionized water and also in boiling water
- The substrates were cleaned ultrasonically for 15 minutes in the stainless steel tank of the ultrasonic agitator containing tricholroethylene
- The substrates were then washed with distilled water
- The substrates were mounted in a specially designed holder and kept over a beaker that contains isopropyl alcohol

- The alcohol is heated so that the substrates will be cleaned by the vapor degreasing process
- Later, the substrates were subjected to ultrasonic agitation with a detergent followed by washing with double distilled water
- Finally, substrates were dried by blowing hot air and transferred to the sputtering chamber.

CHARACTERIZATION OF THIN FILMS

In the present study, the following characterization measurements were undertaken to evaluate the physical properties of the experimental films.

(i) Film thickness

(ii) Film composition

(iii) Crystal structure

(iv) Surface morphology

(v) Electrical properties and

(vi) Optical properties

2.7 Film thickness measurement

The optical interference methods were used to determine the thickness of the deposited films. The Tolansk's multiple beam interference method [38] was employed for the measurement of the films thickness. The Hitachi U3400 UV-Vis-NIR double beam spectrophotometer was used to record the optical transmittance spectra. The thickness of the experimental films was also determined by the interference fringes of the

transmittance with an accuracy of ± 1%. The thickness (t) of the film was estimated using the relation [37],

$$\text{Thickness (t)} = \frac{m\lambda_1\lambda_2}{2n(\lambda_2-\lambda_1)} \quad [\text{nm}] \qquad \text{-----(4)}$$

where 'm' is the order of interference, λ_1 and λ_2 are the wavelengths corresponding to the two successive maxima and minima of the transmittance spectrum respectively and 'n' is the corresponding refractive index.

2.8 Composition analysis

The composition of the experimental films was analyzed using X-ray photoelectron spectroscopy (XPS). X-ray photoelectron spectroscopy is also known as electron spectroscopy for chemical analysis (ESCA) is accomplished by irradiating a sample with monoenergetic soft X-rays and analyzing the energy of the emitted electrons. Mg K_α X-rays (1253.6eV) or Al K_α X-rays (1486.6eV) are ordinarily used. These photons have limited penetrating power in solid. They interact with atoms in this surface region causing electron emition as per the photoelectric effect. The emitted electrons have kinetic energies given by the relation [39],

$$KE = h\nu - BE - q\phi_{sp} \qquad \text{-----(5)}$$

Where hν is the energy of the photon, BE is the binding energy of the atomic orbital from which the electron originates, and $q\phi_{sp}$ the work function of the spectrometer. The kinetic energy of the escaping photoelectrons limits the depth from which it can emerge, giving XPS as high surface sensitivity with sampling depth of a few nanometers. Photoelectrons

are collected and analyzed by the instrument to produce a spectrum of emission intensity versus electron binding energy. Since each element has a unique set of binding energies, XPS can be used to identify the elements on the surface. Also, peak areas at nominal binding energies can be used to quantify concentration of the elements. Small shifts in these binding energies (chemical shifts) provide powerful information about sample chemical states and short-range chemistry.

2.9 Structural analysis

The structural studies of the experimental films were analyzed using X-ray diffraction. X-ray diffractometry is the most widely used characterization technique for the determination of crystallographic structure of the films. It gives the information regarding the lattice parameters, crystal structure, orientation, defects, crystallite size and stresses if any present in the films. In this investigation, Siefert X-ray diffractometer (model 3003TT) with CuK_α radiation source (wavelength, $\lambda = 1.542$ A°) was used for studying the crystallographic structure of the deposited films (Fig.2.7). The X-ray source was scanned over the film in the 2θ range of 10-80°. The X-ray generator was operated at 40 kV and 30 mA. From the XRD profiles the interplanar spacing 'd' was calculated using the Bragg's relation [40],

$$2d \sin\theta = n\lambda \qquad \text{-----(6)}$$

where 'n' is the order of the diffraction, 'λ' is the wavelength of X-rays and 'θ' is the diffraction angle.

The lattice planes (hkl) were identified (from the JCPDS data) and the lattice constants of the deposited films were determined using the relations [41,42].

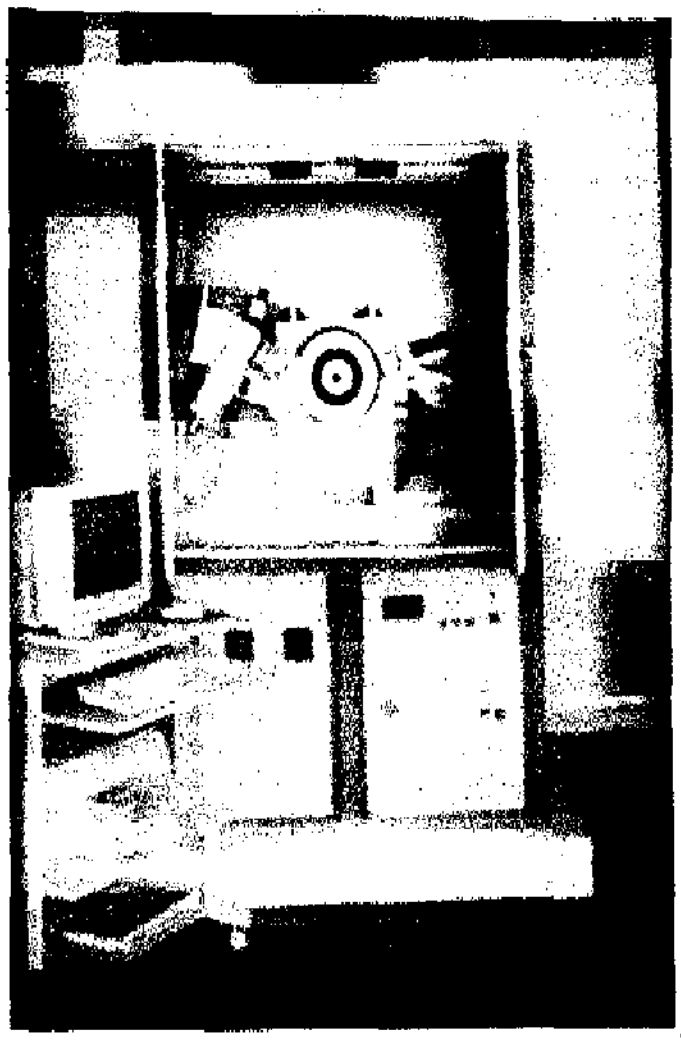

Fig. 2.7 X-ray diffractometer (model Siefert 3003TT)

For cubic structure

$$d = \frac{a}{(h^2 + k^2 + l^2)^{1/2}} \quad [nm] \qquad \text{---(7)}$$

Rombohedreal structure

$$d^2 = \frac{(h^2+k^2+l^2)\sin^2\alpha + 2(hk + kl + lh)(\cos^2\alpha - \cos\alpha)}{a^2(1-3\cos^2\alpha + 2\cos^3\alpha)} \quad [nm] \qquad \text{-----(8)}$$

For hexagonal structure

$$d^2 = \frac{4}{3}\left(\frac{h^2+hk+k^2}{a^2}\right) + \frac{l^2}{c^2} \quad [nm] \qquad \text{-----(9)}$$

The crystalline size (L) of the films was calculated using the Scherrer's equation [40]

$$L = \frac{k\lambda}{\beta\cos\theta} \quad [nm] \qquad \text{-----(10)}$$

where 'k' a constant with a value about 0.89 for Cu target, 'β' is the full width at half maximum (FWHM) intensity of the peak measured in radians.

The internal stress developed in the films was estimated using the relation [43],

$$\sigma = \frac{-E(a - a_o)}{2\nu a_o} \quad [GPa] \qquad \text{----(11)}$$

where 'E' is the Young's Modules of the sample (Cu_2O = 30 GPa), 'a' is the lattice parameter of the bulk material, 'a_o' is the measured lattice parameter and 'ν' is the Poisson's ratio (Cu_2O = 0.455).of the sample.

2.10 Surface morphology

The surface morphology and topography of the films were studies using scanning electron microscope and atomic force microscopy.

Scanning electron microscope (SEM)

The Scanning Electron Microscope (SEM) is designed for the direct studying of the surface topography and grain size of the film. By scanning the sample with an

electron beam that has been generated and focused by the operation of the microscope, and the image is formed. The SEM allows a grater depth of focus than that of the optical microscope. For this reason the SEM can produce an image that is good representation of three-dimensional appearance of the sample image. A thin layer of gold is deposited on the film surface to avoid charging problems. In the present study, a Hitachi SEM model S: 4000 was used to obtain micro-structural features of the films.

Atomic force microscope (AFM)

Atomic Force Microscope (AFM) is one of the foremost powerful tool for the analysis of the surface morphology of thin films. The AFM has several advantages over the electom microscope. Unlike the electron microscope which provides a two-dimensional projection or a two-dimensional image of a sample, the AFM provides a true three-dimensional surface profile. Additionally, samples viewed by an AFM do not require any special treatment that would actually destroy the sample and prevent its re-use. This technique can also be extended for the determination of the topography of almost all kinds of surfaces and can operate in different media like air, liquid and vacuum. The AFM utilises a sharp probe moving over the surface of a sample in a raster scan. In case of the AFM, the probe is a tip on the end of a cantilever, which bends in response to the force between the tip and the sample. The basic technology involved in the AFM is the sample motion using piezoelectric transducers, feedback controller, image handling, vibration damping etc. The critical part of the AFM is the force sensor, which transforms the force interaction over the tip-sample junction to an electrical signal that can be handled by the feedback electronics. This is done by mounting the tip on a

flexible cantilever combined with a deflection sensor that can measure the cantilever motion as the tip interacts with the surface. As the tip is a part of the force sensor, it is normally the sample that is moved with a piezoelectric transducer in the AFM.

In the present investigation, Digital Instruments AFM Nanoscope III was used for obtaining the images of the grown films. The surface of the films is scanned over an area of 10 μm x 10 μm. The grain size and the surface roughness of the samples are studied in order to get the morphological data.

2.11 Electrical characterization

The electrical resistivity and the Hall mobility analysis give the transport behavior of semiconductors. Such analysis make it possible to determine the type of charge carriers, carrier concentration, carrier mobility and transport mechanism of the carriers present in the films.

The electrical resistivity and the Hall effect measurements on the sputter Cu_2O and $CuAlO_2$ films were carried out using the van der Pauw technique [44]. The experimental set up of Hall effect measurements is shown in Fig.2.8. An electrical current in the range 1μA – 10 mA and a magnetic field strength of 8,000 Gauss were applied to the sample. Advantest programmable dc voltage/current generator (model TR 6142) was employed to pass current through the sample and it was measured using Keithley (model 160 B) digital multimeter with accuracy of 1 nA. The potential drop across the sample

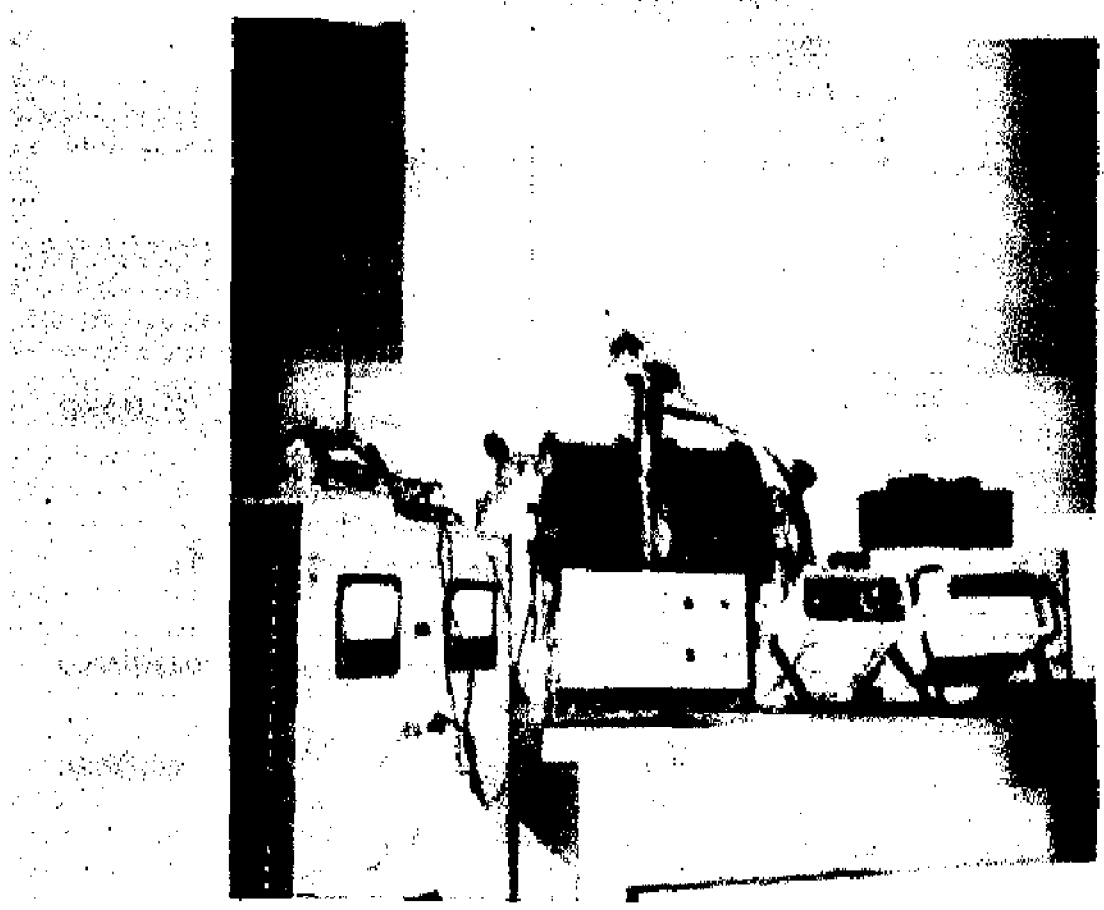

Fig.2.8 shows the experimental set up of Hall effect

was measured with Solartron computing voltmeter (model 7071) with an accuracy of ± 1 μV. In order to avoid the thermoelectric and thermomagnetic effects, the polarity of the current was reversed during each measurement and the average values were taken.

The sheet resistance (R_S) of the experimental film was calculated using the relation [45],

$$R_S = \frac{\pi}{\ln 2} f \frac{R_1 + R_2}{2} \quad [\Omega/\square] \qquad \text{---(12)}$$

where, 'f' is the van der Pauw correction factor

$$f = 1 - \frac{\ln 2}{2}\left(\frac{R_1 - R_2}{R_1 + R_2}\right)^2 \qquad \text{---(13)}$$

The electrical resistivity (ρ) of the experimental films was evaluated using the relation,

$$\rho = R_S \cdot t \qquad [\Omega\,cm] \qquad \text{-----(14)}$$

where, 't' is the thickness of the experimental film.

The Hall parameters of the experimental films such as Hall mobility (μ_H), Hall co-efficient (R_H) and carrier concentration (n) were determined using the following relations

$$\mu_H = \frac{10^8 \times \Delta R}{B.R_S} \qquad [cm^2/Vsec] \qquad \text{-----(15)}$$

$$R_H = \mu_H \rho \qquad [cm^3 coulomb^{-1}] \qquad \text{-----(16)}$$

$$n = \frac{1}{R_H . e} \qquad [cm^{-3}] \qquad \text{-----(17)}$$

where 10^8 is the conversion factor from electrostatic units to experimental units, 'B' is the applied magnetic field strength, 'ΔR' is the change in resistance calculated from the developed Hall voltage film and 'e' is the charge of the electron.

2.12 Optical characterization

In the present study the Cu_2O and $CuAlO_2$ films were optically characterized to determine the absorption coefficient, optical transmittance, optical band gap, Refractive index and Extinction coefficient.

The optical transmittance and reflectance of the films were recorded using a Hitachi (model U 3400) UV-Vis-NIR *double beam* spectrophotometer (as shown in Fig.2.9). It is a sophisticated and advanced computer controlled instrument with an accuracy of ± 0.2 nm in UV-Vis region and ± 1nm in the near infrared (NIR) region.

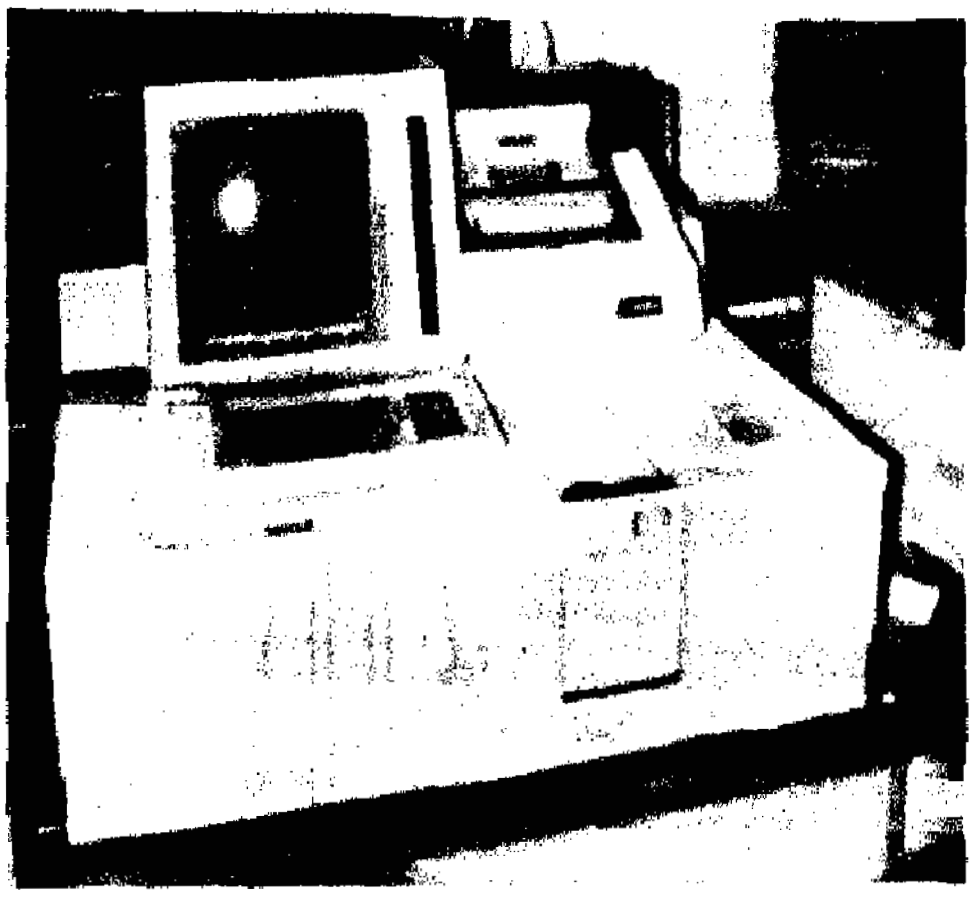

Fig. 2.9 The photograph of the Hitachi U:3400 spectrophotometer

Deuterium (D_2) and iodine tungsten (W_1) lamps were used as the sources of light in the UV-Vis region and NIR region, respectively. The block diagram of the optical system of the Hitachi U:3400 spectrophotometer is shown in Fig.2.10. The light coming from two sources is reflected by mirrors and then passed through the monochromators and prism for the dispersion of light (spread into spectrum). Then a particular wavelength based on the requirement from the dispersed light was selected and passed it through the rotating mirrors, which directs the light beam alternatively through the sample and

reference. These two light beams converge on the detector. The relative intensities of the two beams that strike the detector provide a measure of the amount of light absorbed or transmitted by the sample. The measured optical absorption and/or transmittance of

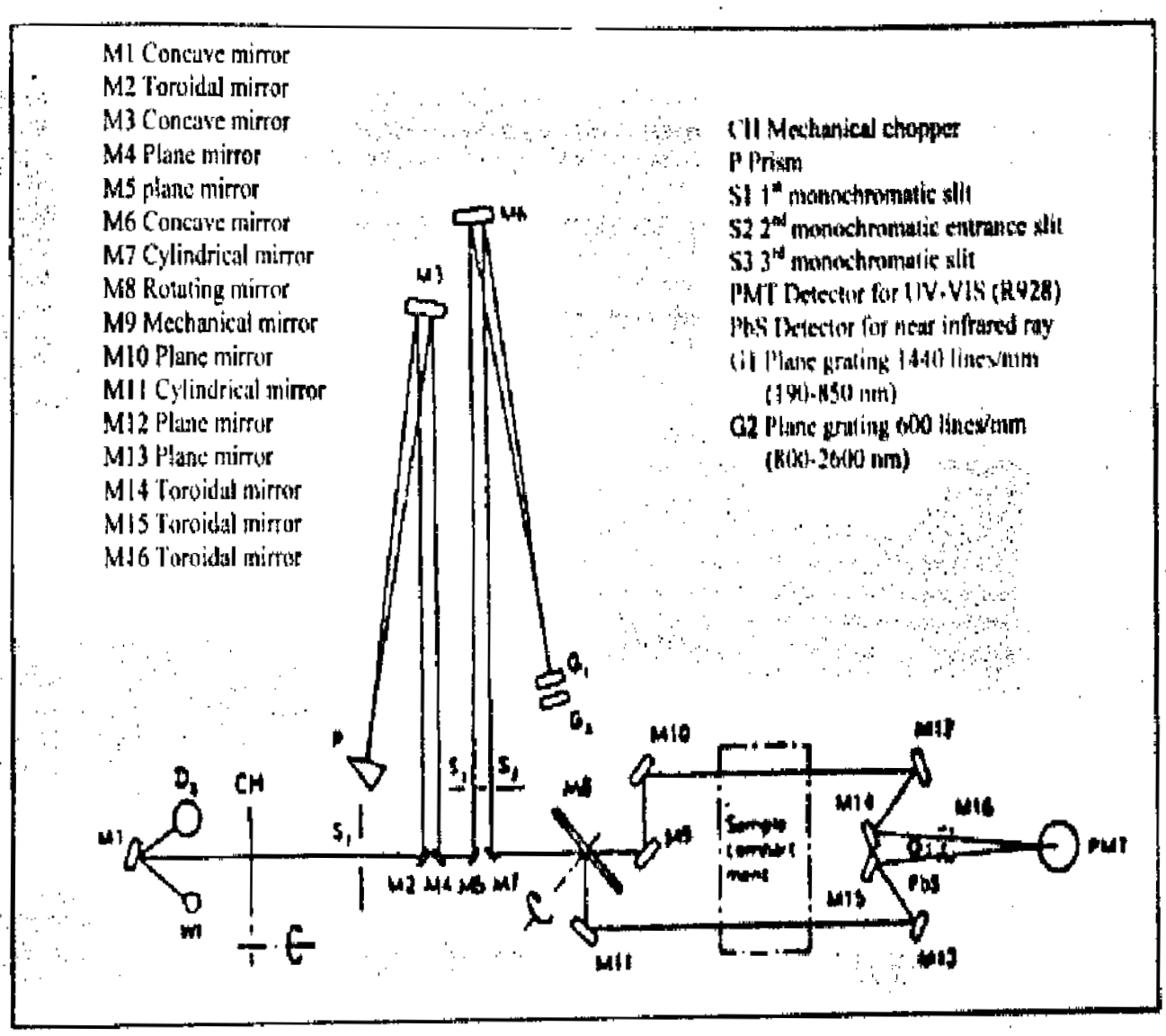

Fig.2.10 The block diagram of the optical system of the Hitachi U:3400 spectrophotometer

the given sample is directly displayed on the monitor of the spectrophotometer as a function of wavelength. This spectrum is recorded using a plotter, which is attached to the instrument.

The Optical absorption coefficient (α), which is the relative rate of decrease in light intensity along its path of propagation, was evaluated using the relation,

$$\alpha = \frac{1}{t} \ln \frac{T}{(1-R)^2} \quad [cm^{-1}] \qquad \text{-----(18)}$$

where 'T' is the transmittance, 'R' is the reflectance and 't' is the thickness of the film.

The optical transitions between the valance and conduction bands of a semiconductor can be understood by studying the dependence of α on photon energy (hν). For various types of optical transitions, the absorption coefficient Cu_2O obeys the relation [46],

$$\alpha h\nu = A (h\nu - E_g)^n \qquad \text{-----(19)}$$

$\alpha h\nu = A (h\nu - E_g)^{1/2}$ for direct allowed transition,

$\alpha h\nu = A (h\nu - E_g)^{3/2}$ for direct forbidden allowed transition,

$\alpha h\nu = A (h\nu - E_g)^2$ for indirect allowed transition, and

$\alpha h\nu = A (h\nu - E_g)^3$ for indirect forbidden allowed transition,

where 'A' is the edge width parameter. 'E_g' is the optical band gap.

The intercept on the x-axis of the linear region of the extrapolated plot of $(\alpha h\nu)^2$ versus hν gives the value of E_g.

The refractive index n(λ) and extinction coefficient k(λ) of the films were calculated using the Swanepoel's envelope method [47] from the transmittance spectra. The transmittance maxima T_M (λ) and Minima T_m (λ) at various wavelengths were read from the envelope and used for the determination of the optical constants. The refractive index of the films (n) was determined using the relation,

$$n(\lambda) = [\, N + (N^2 - n_o^2\, n_l^2)^{1/2}]^{1/2} \qquad \text{-----(20)}$$

$$N = 2n_0n_l \frac{T_M - T_m}{T_M\, T_m} + \frac{n_o^2 + n_l^2}{2} \qquad \text{-----(21)}$$

Where n_o and n_l are the refractive indices of air and the substrate respectively.

The extinction coefficient (k) was determined using the relation [48],

$$k = \frac{\alpha\lambda}{4\pi} \qquad \text{-----(22)}$$

2.13 Figure of Merit

Optical transmittance and the electrical conductivity are the two important parameters with which the quality of the transparent conducting oxides (TCOs) is judged. These two parameters are somewhat inversely related. A method of comparing the properties of TCO by means of figure of merit (F) was developed.

The figure of merit of $CuAlO_2$ films was calculated using the relation [49],

$$F = \frac{-1}{(\rho \ln T)} \quad [\Omega^{-1}cm^{-1}] \qquad \text{-----(23)}$$

Where 'ρ' is the electrical resistivity and 'T' is the average optical transmittance in the wavelength region between 400 -1600 nm. A film with low electrical resistivity and high optical transmittance leads to a relatively high figure of merit.

References

[1] R.W. Berres, P.M. Hall and M.T. Harris
Thin Film Technology, Van Nostrand, Princeton New Jersey, (1968).

[2] R.F. Bunshah
"Deposition Technologies for Films and Coatings", Noyes Publications, New Jersey, (1982).

[3] K.L. Chopra
"Thin Film Phenomena", Ml Graw-Hill, New York, (1969).

[4] L.I. Maissel and R. Glang
"Handbook of Thin Film Technology", Ml Graw-Hill, New York, (1970).

[5] J. George
"Preparation of Thin Films", Marcel Dekker, New York, (1992).

[6] N. Tabuchi and H. Matsumura
Jpn. J. Appl. Phys., 41 (2002) 5060.

[7] T. Mahalingam, J.S.P. Chitra, J.P. Chu and P.J. Sebastian
Solar Energy Mater& Solar cells, 88 (2005) 209.

[8] J. Morales, L. Sanchez, S. Bijani, L. Martinez, M. Gabas and J.R.R. Barrado
Electochemical Solid State Letters, 8 (2005) 159.

[9] M. Yang and J.J. Zhu
J. Cryst. Growth, 256 (2003) 134.

[10] S.C. Ray
Solar Energy Mater & Solar Cells, 68 (2001) 3071.

[11] M. Ristov and G.J. Sinadenovski
Thin Solid Films, 123 (1985) 63.

[12] J.H. Ho and R.W. Vook
Phil. Mag., 36 (1997) 105.

[13] D.S. Kim and S.Y. Choi
Phys. Stat. Solidi (a), 202 (2005) R 167.

[14] T. Maruyama
Jpn. J. Appl. Phys., 37 (1998) 4099.

[15] H. Gong, Y. Wang and Y. Luo
Chemical Vapour Deposition, 76 (2000) 3959.

[16] Z.H. Gan, G.Q. Yu, B.K. Tay, C.M. Tan, Z.W. Zhao and Y.Q. Fu,
J. Phys D: Appl. Phys., 37 (2004) 81.

[17] H. Kawazoe, M. Yasukawa, H. Hyodo, M. Kurita, H. Yanagi and H. Hosono
Nature, 389 (1997) 939.

[18] N. Kikuchi and K. Tonooka
Thin Solid Films, 486 (2005) 33.

[19] B. Balamurugan, B.R. Mehta, D.K. Avasthi, G. Singh, A.K. Arora,
M. Rajalakshmi, G. Raghavan, A.K. Tyagi and S.M. Shivaprasad
J. Appl. Phys., 92 (2002) 3304.

[20] K. Tonooka, K. Shimokawa and O. Nishimura
Thin Solid Films, 411 (2002) 129.

[21] S. Gao, Y. Zhao, P. Gao, N. Chen and Y. Xie
Nonotechnology, 14 (2003) 538.

[22] A.N. Banerjee, C.K. Ghosh and K.K. Chattopadhyay
Solar Energy Mater & Solar Cells, 89 (2005) 75.

[23] N. Tsuboi, Y. Takahashi, S. Kobayashi, H. Shimizu, K. Kato and F. Kaneko
J. Phy & Chem. Solids, 64 (2003) 1671.

[24] J.F. Pierson, D. Wiederkehr and A. Billard
Thin Solid Films, 478 (2005) 196.

[25] S. Ishizuka, K. Suzuki, Y. Okamoto, M. Yanagita, T. Sakurai, K. Akimoto,
N. Fujiwara, H. Kobayashi, K. Matsubara and S. Niki
Phys. Stat. Solidi (c), 1 (2004) 1067.

[26] W.R. Grove
Phil. Trans. Faraday Soc., 87 (1852).

[27] L.I. Maissel
"Physics of Thin Films", Vol. 3 (Eds. G. Hass and R.E. Thum,), Academic Press,
New York, 1966.

[28] F.M. Penning
Physica, 873 (1936).

[29] A.S. Penfold and J.A. Thornton
US. Patents 3,884, 793 (1975); 3, 995, 187, 4, 030, 996, 4, 031, 424 and 4, 041, 353 (1977).

[30] J.S. Chapin
Resarch Dev., 25 (1974) 37.

[31] I.G. Kesaer and V.V. Pashkova
Sov, Phys. Tech. Phys., 4: (1959) 254.

[32] F.A. Green and B.N. Chapman
J. Vac. Sci. Technol., 13 (1976) 165.

[33] J.S. Logan, F. Jones, J. Costable and J.E. Lousie
J. Vac. Sci. Tech. A, 5 (1987) 1879.

[34] W.D. Westwood
"Sputter Deposition", AVS, 120 Wall Street, 32nd Floor, New York, NY 10005, 2003, p. 204.

[35] G. Perny and B. Lavelle Saint Martin
"Basic Problems in Thin Films Physics", Ed. R. Niedermayer and H. Mayer Vandernhook and Ruprecent, Gotingsen, (1966) p 709.

[36] J.A. Thornton and A.S. Penfold
"Thin Film Processes", Ed. J.L. Vossen and W. Kern, Academic Press, (1978) p. 75.

[37] S. Tolansky
"Multiple Beam Interferometry of Surfaces and Films", Oxford Press, New York (1948).

[38] J.C. Manifacier, M. De Murcia, J.P. Fillard and E. Vicario
Thin Solid Films, 41 (1997) 127.

[39] C.S. Fadley
"Basic concept in X-ray powder studies in Electron spectroscopy: Theory; Techniques and Applications", (Eds. C.R.Brumelle and A.D. Baker,) Acadomic Press, New York, (1978) p. 2-150.

[40] B.D. Cullity
"Elements of X-ray Diffraction", 2nd Edn. Addition-Wesely, Reading, MA (1978).

[41] L.V. Azaroff and M.J. Buerger
Powder Method of X-ray Crystallography Mc Graw-Hill, New York, (1977).

[42] C.W. Bunn
"Chemical Crystallography", Oxford Univ. Oxford, (1961).

[43] L. Eckertova
"Physics of Thin Films", (New York and London: Plenum press) (1984).

[44] L.J. van der Pauw
Philips Res. Rep., 13 (1958)1.

[45] K.L. Chopra
"Thin Film Phenomena", (New York and London: McGraw Hill), (1969).

[46] J. Tauc
"Amorphous and Liquid Semiconductors", Plenum Press, New York, (1974).

[47] R. Swanepoel
J. Phys. E. Sci. Instrum., 16 (1983) 1214.

[48] M. Born and E. Wolt
"Principle of optics", 3rd ref. Ed. Pergamon Press. Oxford (1961).

[49] P.S. Reddy, G.R. Chetty, S. Uthanna, B.S. Naidu and P.J. Reddy
Solid State Commun., 77 (1991) 899.